Nanoscale

Cite this: *Nanoscale*, 2011, **3**, 1717

www.rsc.org/nanoscale

PAPER

Structural control of gold nanoparticles self-assemblies by layer-by-layer process

Giovanna Machado,*[ad] Adriano F. Feil,*[b] Pedro Migowski,[c] Liane Rossi,[e] Marcelo Giovanela,[f] Janaina da S. Crespo,[f] Leonardo Miotti,[bg] Maurício A. Sortica,[b] Pedro L. Grande,[b] Marcelo B. Pereira[b] and Ricardo R. B. Correia[b]

Received 27th December 2010, Accepted 30th January 2011
DOI: 10.1039/c0nr01023e

This work presents a novel way to introduce gold nanoparticles (Au NPs) in a multilayer polymer produced by the layer-by-layer (LbL) assembling technique. The technique chosen shows that, depending on the pH used, different morphological structures can be obtained from monolayer or bilayer Au NPs. The MEIS and RBS techniques allowed for the modelling of the interface polymer-NPs, as well as the understanding of the interaction of LbL system, when adjusting the pH in weak polyelectrolytes. The process reveals that the optical properties of multilayer systems could be fine-tuned by controlling the addition of metallic nanoparticles, which could also modify specific polarization responses.

Introduction

Nanotechnology has brought new challenges to nanostructures based on inorganic and organic substances. The synthesis of nanoparticles (NPs) has received particular attention due to the interest in their optical and electronic properties.[1] In fact, there is a growing need to enhance the function of these engineered structures beyond their present boundaries through the use of advanced materials. Therefore, gold NPs with diameters ranging from 1 to 100 nm, with unique optical and electronic properties,[2–4] are attractive candidates for the construction of inorganic-organic hybrid structures, which can be applied in advanced spectroscopy, chemical and biosensor technology and micro-electronic devices.[5–7] Different methods of synthesis can be used to prepare metallic NPs. Among them, the layer-by-layer (LbL) processes are notable as a route to obtain NPs of specific size through the colloidal methodology.[8–12] The polyelectrolyte multilayer (PEMs) process, for example, involves deposition of weak electrolytes from a diluted aqueous solution. In this case the ultrathin films are assembled from repetitive and sequential adsorption of oppositely charged polyelectrolytes.[8] The advantage of this process is that these polymers present linear charge densities that can be changed by adjusting the pH of the dipping solution. The pH's adjusting allows the control of the properties such as thickness and roughness in the LbL process.[13–15]

Several works have been developed using the LbL process. Recently it was shown that silver NPs obtained by the reduction of silver acetate ($AgCH_3CO_2$) in ambient UV light induces the formation of Ag NPs with different crystallinity.[16] The reducing method with ambient light formed larger Ag NPs (4–50 nm) in comparison with the reduction method using UV light (2–4 nm).[16] Furthermore, it has been shown that varying the gold NPs shape, size and spacing distribution, the surface plasmon resonance (SPR) peak can be tuned to a wide range of wavelengths.[4,17–21] Moreover, changing the configuration of the arrangement of nanoparticles on the surface, such as the number of NPs layers, can also significantly affect the optical properties of the matrix. The distance between Au NPs and the NPs density per unit area significantly affects the SPR effects. It was revealed that a system with a single layer of nanoparticles showed a peak of extinction in the region of 510–550 nm. The same system with the highest density of NPs and a second extinction peak between 620 and 660 nm was observed. This effect was explained by collective SPR from intralayer interparticle coupling.[2,15] For this kind of layer-by-layer system the combination of optical multilayer films and plasmonic structures allows the design of specific optical responses in photonic devices.[22] The control of these particular optical properties depends not only on the structured layer materials and inclusions, but also on the shape and spatial organisation of the plasmonic elements.[22] The process described demonstrates that the optical properties of multilayer systems could be tuned by the controlled addition of metallic

[a]*Centro de Tecnologias Estratégica do Nordeste – CETENE, Recife, PE, Brazil. E-mail: giovanna@cetene.gov.br; Tel: +55 81 33347200*
[b]*Instituto de Física, Universidade Federal do Rio Grande do Sul – IF-UFRGS, Porto Alegre, RS, Brazil. E-mail: affeil@if.ufrgs.br; Tel: +55 51 3308 6457*
[c]*Instituto de Química, Universidade Federal do Rio Grande do Sul – IQ-UFRGS, Porto Alegre, RS, Brazil*
[d]*Universidade Federal de Pernambuco – UFPE, Recife, PE, Brazil*
[e]*Instituto de Química, Universidade de São Paulo – IQ-USP, São Paulo, SP, Brazil*
[f]*Universidade de Caxias do Sul – UCS, Caxias do Sul, RS, Brazil*
[g]*Department of Physics, North Carolina State University, Raleigh, North Carolina, USA*

nanoparticles, which could also modify specific polarization responses.

In this context, the aim of this work was to study the diffusion process of gold NPs in the PEM films in order to control the nanostructures to produce gold NP self assemblies for optical applications. The medium energy ion scattering (MEIS) and Rutherford backscattering spectroscopy (RBS) techniques allowed modelling the interface polymer-NPs as well as understanding the interaction of the LbL system by adjusting pHs in weak polyelectrolytes.

Experimental section

Preparation of gold nanoparticles by LbL

For the preparation of the sample three different substrates were used (glass, polystyrene, silicon wafer). These substrates were immersed in cationic and anionic polymer solutions. Poly(allylamine hydrochloride) (PAH) (Mw 70,000) (Sigma–Aldrich) was used as polycations, while poly(acrylic acid) (PAA) (Mw 90,000, 25% aqueous solution) (Polysciences) was used as the polyanion. All polyelectrolytes were utilised as received without any kind purification. PAH and PAA were prepared as 0.01M solutions (based on the repeat-unit molecular weight). The polyelectrolyte solutions were adjusted to the desired pH (± 0.01) with 1M HCl or 1M NaOH.

The substrate was immersed into the polycation aqueous solution (PAH) for 15 minutes followed by rinsing once in pure water for 1 min, and then twice for 2 min. The polycation adsorbed substrate was then dipped into the polyanion solution (PAA) for 15 minutes and then rinsed with water. The rinsing step was repeated at least two times.

The films were prepared for combinatorial experiments: $(PAH_{3.5}/PAA_{3.5})_{20}$, $(PAH_{7.5}/PAA_{3.5})_{20}$, where 3.5 and 7.5 are the pH of the PEM solution and 20 is the number of bilayers, as can be seen in Fig. 1a.

These PEMs were immersed in a gold colloidal solution (pH 3.0 and 6.0) for 1 h and then removed and rinsed in deionized water three times for 1 min, the pH was adjusted with 1M HCl. The Au NPs were synthesised by the classical citrate method.[23] Fig. 1b shows the final structure of Au NPs stabilised with a negative charge.

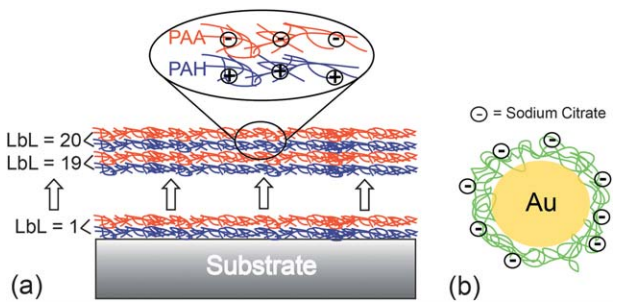

Fig. 1 (a) Schematic of the synthesis of the 20 layers of LbL using PAH/PAA. In the detail a representation of how the distributions are loads on the LbL surface. (b) Schematic configuration of a gold nanoparticle stabilised with citrate, indicating that the surface charge is negative.

Nanoparticles characterization

The morphology and roughness of the multilayers films were characterised by atomic force microscopy (AFM). The AFM measurements were performed in air using the tapping mode (Dimension 3000 Veeco Instruments). For transmission electron microscopy the multilayer films were deposited on polystyrene (PS) coverslip substrates. This material was then immersed in a gold colloidal solution. Afterwards, thin strips of PS coverslip samples were cut and embedded in an epoxy resin that was cured at 50 °C for 48 h. The embedded specimens were first trimmed with a glass knife and then ultrathin cross sections were obtained using a cryogenic Diatome diamond knife at a 45° angle at room temperature. The ultrathin sections of approximately 80 nm thickness were floated on a deionized water surface and immediately mounted onto 200 mesh copper grids and dried in a desiccator. Finally they were examined using a JEOL 200CX TEM operating at an accelerating voltage of 120 kV.

RBS analysis was conducted using alpha particles ($^4He^+$ ions) with 1.4 MeV energy with normal incidence and 165° detection. Gold quantification was carried by comparison with a standard reference implanted with 1×10^{16} cm^{-2} Au atoms.[4] MEIS analysis was performed with a beam of H^+ ions with 100 keV of energy with normal incidence and a scattering angle in the range of 108° to 132°. The MEIS experimental spectra was fitted with the software PowerMeis.

The UV–visible absorption spectra were recorded from samples deposited on 1 mm thick optical glass substrates on a Cary 5000 spectrophotometer varying in the range 350–750 nm. In order to investigate the distribution of gold NPs additional optical measurements were performed using spectral ellipsometry (SE), which is one of the most powerful tools to investigate the optical properties of materials.[24,25]

The measurements were performed using a spectral ellipsometer SOPRA GES-5E with microspot accessory (numerical aperture of 3°) that focuses the light beam in a small region of the film surface (approximately 365 μm × 270 μm). All measurements were made at an angle of incidence of 68° and in a wavelength range of 300–850 nm.

Results and discussions

Self-assemblies of gold nanoparticles

In Fig. 2 the TEM, AFM images and the histogram distribution size of Au NPs for different PEM films are displayed. The Table 1 shows the dispersion of the Au NPs deposited in the PEMs for different pHs. The following will discuss systems $(PAH_{7.5}/PAA_{3.5})_{20}$ and $(PAH_{3.5}/PAA_{3.5})_{20}$ for the colloidal gold solution at pH 3.0 and 6.0.

In the PEM films $(PAH_{7.5}/PAA_{3.5})_{20}$ the variation of the Au NPs pH from 6.0 (S1) to 3.0 (S3) changed the amount of NPs on the polyelectrolyte multilayer. It means that for system $(PAH_{7.5}/PAA_{3.5})_{20}$ the PAA chains are adsorbed at a low pH and a low ionization degree onto charged chains of PAH. On one hand when the system is immersed in gold solution pH = 6.0 the surface layers have a major charge density yielding a surface enriched with Au NPs and it is possible to verify a bilayer of Au NPs on the top surface (S1).

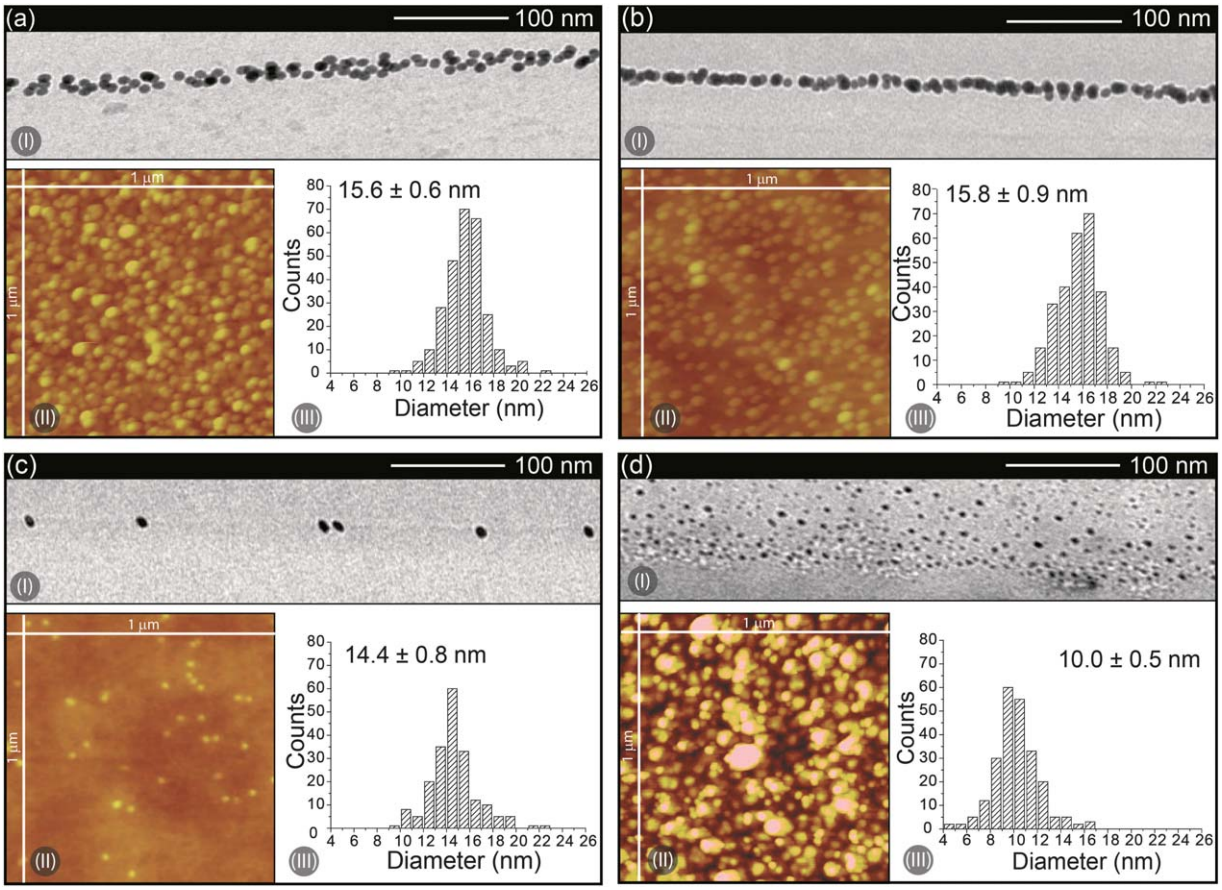

Fig. 2 Sequence of four different LbL systems, where (a) S1, (b) S2, (c) S3 and (d) S4 matching the figures of TEM (I), AFM (II) and histogram distribution size (III).

Table 1 Sample nomenclature for different pHs of PEM films immersed in Au NPs

Sample	PAH (pH)	PAA (pH)	Au (pH)
S1	7.5	3.5	6.0
S2	3.5	3.5	3.0
S3	7.5	3.5	3.0
S4	3.5	3.5	6.0

The reason why of this effect is that amines groups are partially ionized and, consequently, negative charge of Au NPs can block the NPs diffusion due to electrostatic repulsion of these NPs with the amines group, resulting in a superficial bilayer of Au NPs (see Fig. 2a).

On the other hand, when the system is immersed in gold solution pH = 3.0 the amine groups as well as Au NPs (stabilised by sodium citrate) are partially ionized, prejudicing the adsorption or diffusion of these NPs on PEM.

Its response is illustrated in Fig. 2c (S3) - where can be observed a incomplete monolayer formed by a reduced number of Au NPs on their surface.

In the case of the multilayer thin films $(PAH_{3.5}/PAA_{3.5})_{20}$ the PAH chains are fully ionized at this low pH, while for PAA the chains are adsorbed at low degrees of ionization. However, when the system is immersed in gold solution pH = 3.0 (S2) a compact monolayer of Au NPs is verified on the top surface (see Fig. 2b). The comportament observed is a consequence of the neutralization of the citrate ions at pH 3.0, since the carboxylate anions are mostly protonated decreasing the surface charge of the Au NPs, which can compromise their ability to interact with the PAH chains. However, it is verified that Au NPs homogeneously distribute through PEM (see Fig. 2d) for samples immersed in gold solution pH = 6.0 (S4). The diffusion of Au NPs is a function of the ionization degree of the PAH during the PEM assembling procedure, because amine groups are fully charged and consequentely Au NPs tend to diffuse towards the amine groups that are not totally conjugated to the carboxylic acid.

RBS and MEIS analysis

The RBS and MEIS analyses were used to assess the relative amount and size of the Au NPs layer formed by the LbL process. Fig. 3a shows the RBS spectra of samples S1, S2, S3 and S4 on glass substrates. It is possible to identify elements such as Ca, Si, O and C typically found in soda-lime glass. The area of the Au peak directly gives the amount of Au atoms per unit area, see Fig. 3b. Through a standard sample with 1×10^{16} atoms.cm^{-2} Au it was possible to measure the number of Au NPs on the LbL surface. It was observed that samples S1, S2, S3 and S4 have 4.83×10^{15}, 4.5×10^{15}, 1.22×10^{15} and 8.81×10^{13} atoms cm^{-2}, respectively. These results identify an important difference in the

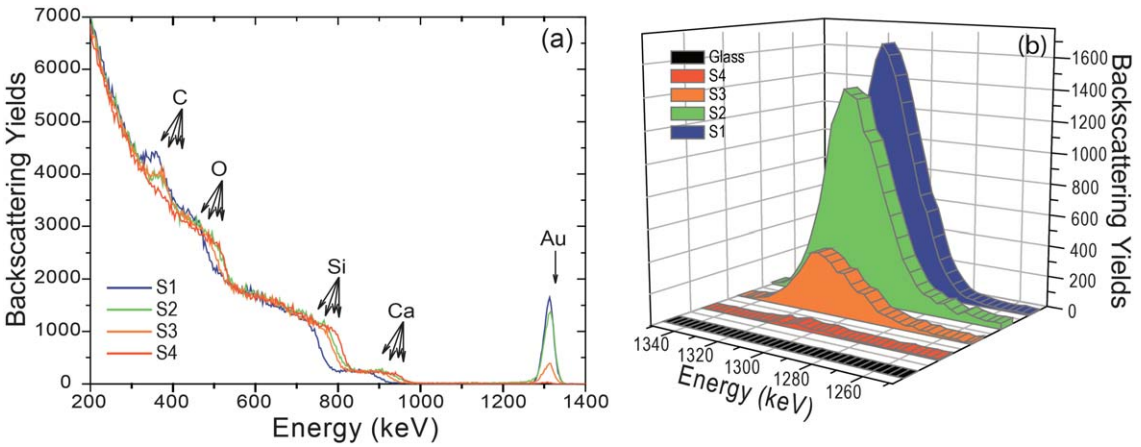

Fig. 3 (a) RBS spectra of samples S1, S2, S3 and S4 identifying the backscattering signals from Au, Ca, Si, O and C and (b) a detail of Au signal showing the change in the relative concentration of different configurations of LbL.

amount of Au in the samples. The ion scattering techniques such as RBS and MEIS reveal features that are not observed by microscopy techniques. For example, the TEM micrographs, especially Fig. 2d, give an impression that sample S4 has more Au NPs than the other systems, but in fact this sample has the lowest number of Au NPs.

In addition the Au NPs were characterised by a high resolution MEIS technique. This technique has been recently used to characterise nanoparticles, nanoislands and quantum dots exposed on the surface.[26] Basically the nanoparticles' shape, composition, size distribution and stoichiometry can be successfully obtained. Moreover, the first steps for the most

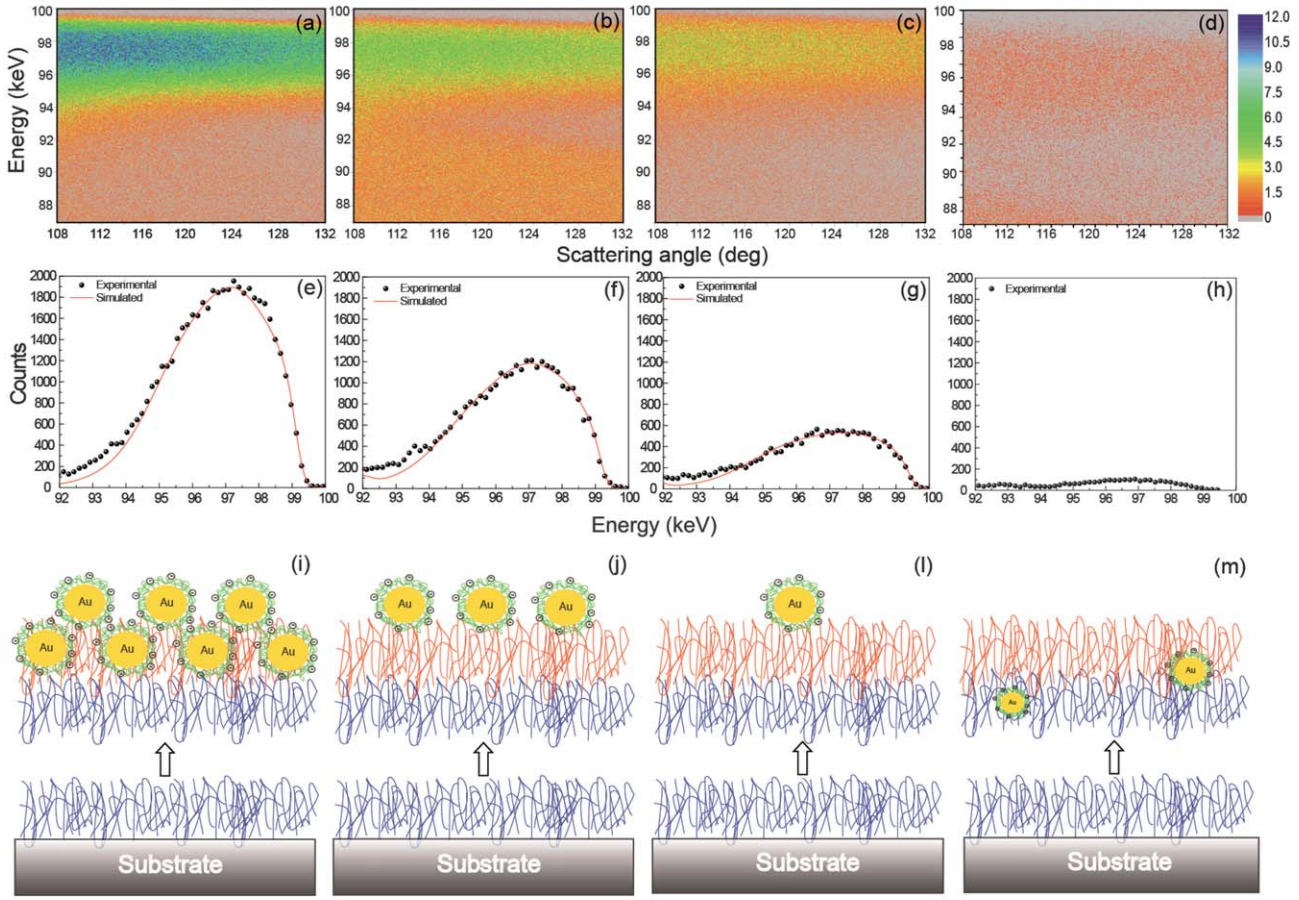

Fig. 4 Sequence of 2D (energy/angle) MEIS spectra (a, b, c and d) and 1D, for a fixed scattering angle of 120 degrees, (e, f, g and h) of the four different LbL systems (samples S1, S2, S3 and S4 described in the text), (i, j, l and m) correspond to NPs configurations that best fit the MEIS results for the samples S1, S2, S3 and S4 respectively.

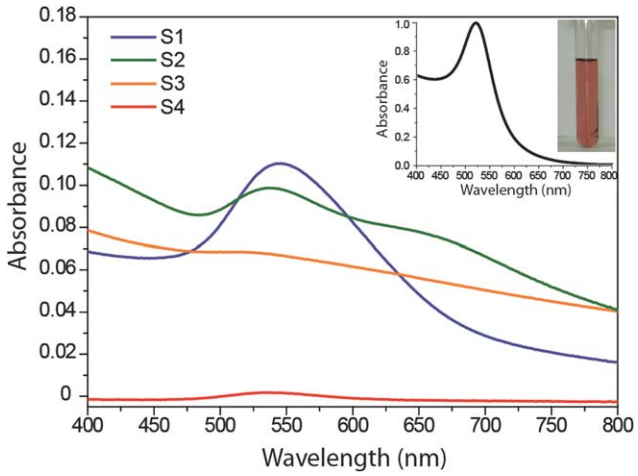

Fig. 5 UV–visible extinction spectrum of the four samples S1, S2, S3 and S4 with different Au NPs self-assemblies.

promising application of MEIS, namely the determination of depth distributions of different elements in a single nanoparticle, have been recently reported.[26–30] Therefore we used the MEIS technique to characterise the NPs distribution on the surface of samples S1, S2 and S3. Figs. 4a–d show sketches representing the samples S1, S2, S3 and S4, respectively. Full Monte-Carlo simulations for the two dimensional map of ion scattering intensities, as a function of the ion scattered energy and angle, were conducted in order to select the best configuration of Au NPs in the samples described here. Figs. 4e–h show the best fitting for samples S1, S2 and S3 using the parameters from Ref. 26. MEIS simulations corroborate with results obtained by TEM in relation to the diameter (see histogram Fig. 2a–d) of Au NPs for samples S1, S2 and S3. For the S1 sample the MEIS results show that the Au NPs are localised inside the first LbL film and under another layer of Au NPs on the surface. This Au NPs bilayer configuration can be seen in Fig. 4i (and TEM images of Fig. 2a). In the case of samples S2 and S3, all Au NPs are adsorbed at the LbL surface forming a Au NP monolayer (Fig. 4j and 4l) with 3.0×10^5 and 3.0×10^4 NP cm^{-2} respectively. Note that the difference in the Au atomic concentration obtained by MEIS analysis for these samples agrees with the RBS results (see Fig. 3b). For sample S4, NPs penetrate deep inside the LbL film and more detailed investigation is needed since the observed low Au concentration prevents any precise MEIS analysis. The model presented helped in the understanding of the diffusional process and structure of Au NPs for the LbL system self-assemblies. Complementary information about the surface of the system (polyelectrolyte and AuNPs) shows that the techniques used are powerful analytical tools in the characterisation of complex nanostructured systems.

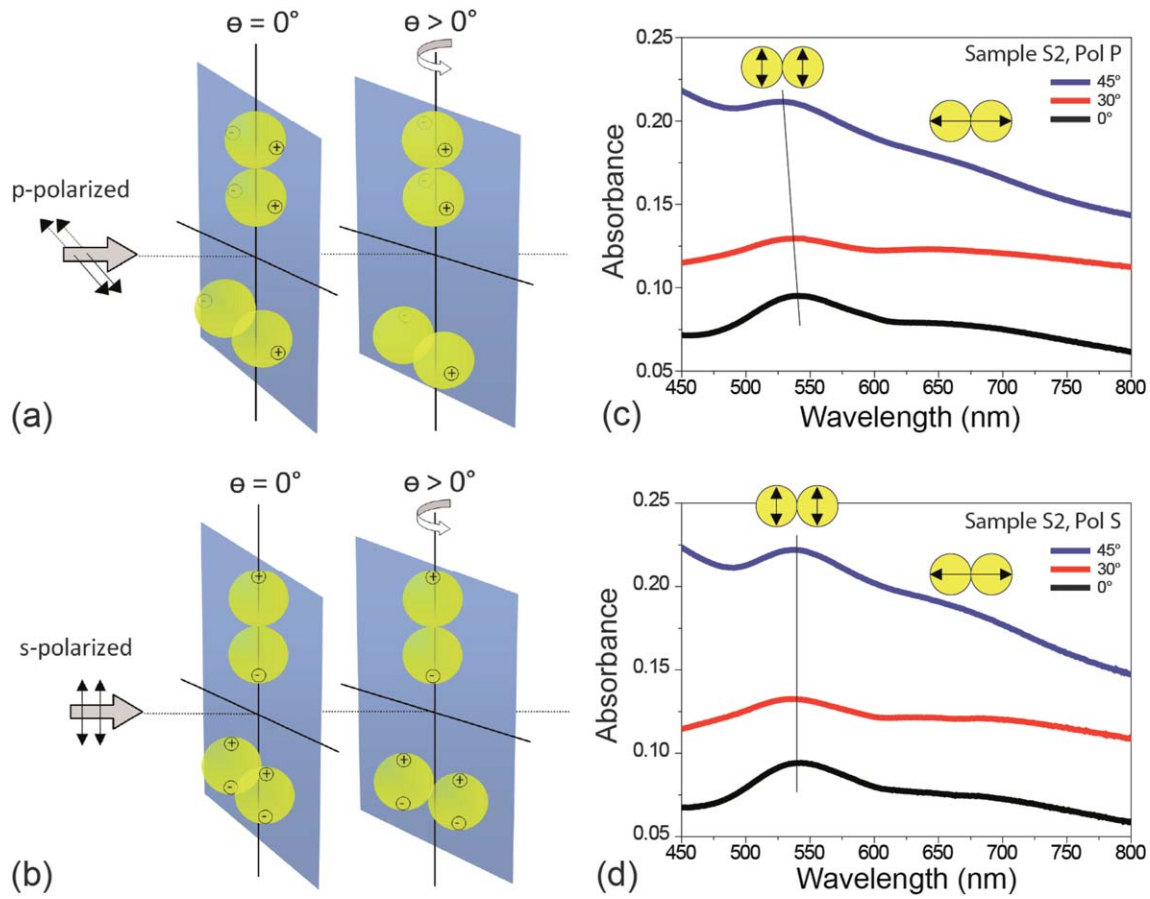

Fig. 6 (a) and (b) Schematic representation of angle-dependent excitation of SPR from intralayer interparticle coupling. (c) and (d) UV–visible extinction spectrum of S2 of the p-polarized and s-polarized light at different incident angles θ, respectively.

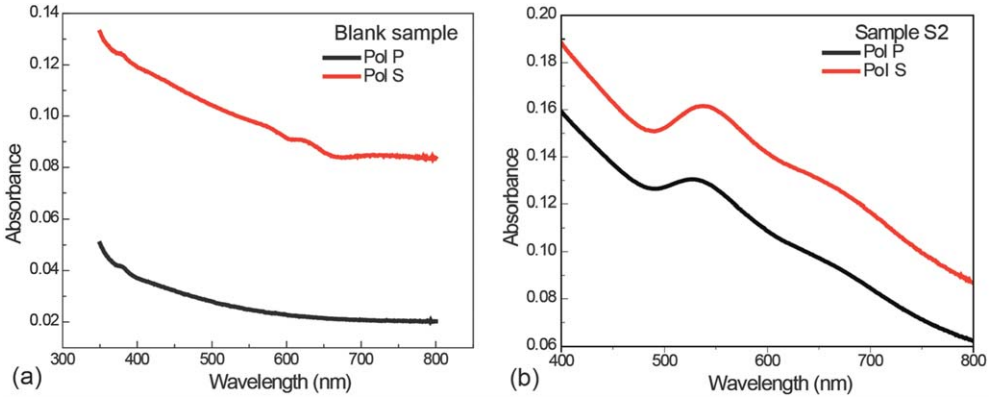

Fig. 7 UV–visible extinction spectrum of the polarizations p and s of (a) blank sample and (b) S2.

Optical properties

The measured UV–visible extinction spectra, taken at normal light incidence, are shown in Fig. 5 for different Au NPs assemblies. Besides the surface plasmon-polariton absorption peak of isolated Au NPs at ~530 nm an additional broad peak close to 650 nm is observed for sample S2.

The polarized measurements at different incident angles were compared with the blank sample as described by Soltwedel *et al.*[22] The Figs. 6a and 6b display the angle-dependent extiction measurement for the sample S2 for p-polarized and s-polarized light, respectively. According to the model of interacting metallic NPs constrained to a plane[22] an optical anisotropy arises due to the compacted structure, observed in Fig. 3b for the same sample. In plane and out of plane the polarizabilities mark the pair wise interaction originating the mode excited along the axis connecting the Au NPs. While s-polarization probes both polarizabilities for all incident angles, the p-polarization selectively excites the out of plane polarizability for grazing incidence.

The Figs. 7a and 7b show the absorption spectra for both S2 and the pure polymer matrix, respectively. Fig. 7a displays additional structures between 600 and 700 nm and shifted SPP resonances of approximately 10 nm for the parallel (p) and perpendicular (s) polarizations with an incidence angle of 45°. This signal must be analysed considering the composition of responses from polymeric and metallic layers. As can be observed in the pure polymer spectra, Fig. 7b, it presents in the extinction for the s-polarization a slight interferometric oscillation between 600–700 nm, which is a fingerprint of the 87 nm polymer thickness. In addition a smooth curve is observed for the p-polarization absorption spectrum at the same wavelength range. Such effect is expected for that polarization, since the p-polarized light would be substantially refracted at air-film interface.

Once the peak is still observed for p-polarized measurements in S2, further measurements were performed using spectral ellipsometry in order to investigate in more detail the anisotropic response of the structure of S2. This technique usually performs analysis of the reflected light polarization state, which is related to the optical properties of the material by the expression:

$$\frac{R_p}{R_s} = \tan(\psi)\exp(i\Delta) \quad (1)$$

The R_P and R_s represent Drude reflectance equations for a thin film (p and s-polarization).[31] The $\tan(\psi)$ and Δ are the amplitude ratio and phase shift difference, respectively, for the p and s-polarization components of light.

Two different analyses were made. First, a pure polymeric film with same thickness as S2 was measured. The spectral curves were analysed with Ellipsometer analysis-modelling software, which assumes isotropic and homogeneous comportament, to perform the best fitting for the S2 and to obtain the dispersion curve and physical thickness of the film.

During these assumptions the best fitting obtained was using Bruggeman's model[32] as an effective medium approximation, with the gold particles partially immersed in the polymer matrix. As a result the film presents a layer of slightly non-spherical gold particles with an effective thickness of $3.2 \times 10^{-3} \pm 3 \times 10^{-4}$ μm and formed by 80% (±2%) of polymer and 20% (±2) of Au NPs.

Conclusions

The dispersion of the NPs in the system LbL can change dramatically depending of pH value in both- colloidal gold solution and PEM films. For the PEM films $(PAH_{7.5}/PAA_{3.5})_{20}$ the variation of the Au NPs pH from 6.0 (S1) to 3.0 (S3) changed the amount of Au NPs on the polyelectrolyte multilayer, respectively forming a compact bilayer and a incomplete monolayer with Au NPs on the LbL surface. When PEM films $(PAH_{3.5}/PAA_{3.5})_{20}$ were immersed in colloidal gold solution at pH 3.0 (S2) a compact monolayer was observed while at pH 6.0 (S4), was verify a homogeneous dissemination of Au NPs through them.

In this context, the changes in pH value of the colloidal gold solution can explain which factors are governing the Au NPs adsorption behavior in the PEM. Nevertheless, the pH of Au colloids is not the only parameter driving the adsorption and diffusion degree of the Au NPs. The assembling procedure of PEM films is also a key parameter on the impregnation of the NPs. In summary we present a novel way to introduce Au NPs in PEM films produced by the LbL assembling technique. The MEIS technique was used to characterise the Au NPs distribution on the surface of samples S1, S2, S3 and S4. The process described showed that the optical properties of multilayer systems could be tuned by the controlled addition of metallic

nanoparticles, which could also modify specific polarization responses.

Acknowledgements

This paper was supported in part by CNPq, CAPES, and FAPERGS Brazilian financial agencies. Parts of this work were carried out in the Department of Chemical Engineering and Department of Materials Science and Engineering, Massachusetts Institute of Technology (MIT), Cambridge, and Robert E. Cohen and Michael F. Rubner are gratefully acknowledged. We also would like to thank Erica Machado for her contribution to this discussion.

References

1 N. Krasteva, I. Besnard, B. Guse, R. E. Bauer, K. Mullen, A. Yasuda and T. Vossmeyer, *Nano Lett.*, 2002, **2**, 551–555.
2 M. C. Daniel and D. Astruc, *Chem. Rev.*, 2004, **104**, 293–346.
3 A. M. Jackson, J. W. Myerson and F. Stellacci, *Nat. Mater.*, 2004, **3**, 330–336.
4 A. F. Feil, P. Migowski, F. R. Scheffer, M. D. Pierozan, R. R. Corsetti, M. Rodrigues, R. P. Pezzi, G. Machado, L. Amaral, S. R. Teixeira, D. E. Weibel and J. Dupont, *J. Braz. Chem. Soc.*, 2010, **21**, 1359–1365.
5 T. Morris, H. Copeland, E. McLinden, S. Wilson and G. Szulczewski, *Langmuir*, 2002, **18**, 7261–7264.
6 Z. S. Wang, T. Sasaki, M. Muramatsu, Y. Ebina, T. Tanaka, L. Z. Wang and M. Watanabe, *Chem. Mater.*, 2003, **15**, 807–812.
7 Y. G. Kim and S. Y. Yang, *J. Nanosci. Nanotechnol.*, 2010, **10**, 6892–6895.
8 G. Decher, *Science*, 1997, **277**, 1232–1237.
9 W. B. Stockton and M. F. Rubner, *Macromolecules*, 1997, **30**, 2717–2725.
10 H. Mattoussi, L. H. Radzilowski, B. O. Dabbousi, E. L. Thomas, M. G. Bawendi and M. F. Rubner, *J. Appl. Phys.*, 1998, **83**, 7965–7974.
11 D. Yoo, S. S. Shiratori and M. F. Rubner, *Macromolecules*, 1998, **31**, 4309–4318.
12 J. D. Mendelsohn, C. J. Barrett, V. V. Chan, A. J. Pal, A. M. Mayes and M. F. Rubner, *Langmuir*, 2000, **16**, 5017–5023.
13 G. Decher and J. D. Hong, *Makromol. Chem., Macromol. Symp.*, 1991, **46**, 321–327.
14 S. S. Shiratori and M. F. Rubner, *Macromolecules*, 2000, **33**, 4213–4219.
15 C. Y. Jiang, S. Markutsya and V. V. Tsukruk, *Langmuir*, 2004, **20**, 882–890.
16 G. Machado, M. M. Beppu, A. F. Feil, C. A. Figueroa, R. R. B. Correia and S. R. Teixeira, *J. Phys. Chem. C*, 2009, **113**, 19005–19010.
17 M. S. Chen and D. W. Goodman, *Science*, 2004, **306**, 252–255.
18 J. S. Ahn, P. T. Hammond, M. F. Rubner and I. Lee, *Colloids Surf., A*, 2005, **259**, 45–53.
19 D. Greshnykh, A. Fromsdorf, H. Weller and C. Klinke, *Nano Lett.*, 2009, **9**, 473–478.
20 N. Sakamoto, H. Ohtsuka, T. Ikeda, K. Maeda, D. L. Lu, M. Kanehara, K. Teramura, T. Teranishi and K. Domen, *Nanoscale*, 2009, **1**, 106–109.
21 M. Hojeij, N. Younan, L. Ribeaucourt and H. H. Girault, *Nanoscale*, 2010, **2**, 1665–1669.
22 O. Soltwedel, O. Ivanova, M. Höhne, M. Gopinadhan and C. A. Helm, *Langmuir*, 2010, **26**, 15219–15228.
23 J. Turkevich, P. C. Stevenson and J. Hillier, *Discuss. Faraday Soc.*, 1951, **11**, 55–75.
24 K. H. Zaininger and A. G. Revesz, *Rca Review*, 1964, **25**, 85–115.
25 J. Goicoechea, C. R. Zamarenno, I. R. Matias and F. J. Arregui, *Sens. Actuators, B*, 2008, **132**, 305–311.
26 M. A. Sortica, P. L. Grande, G. Machado and L. Miotti, *J. Appl. Phys.*, 2009, **106**, 114320.
27 H. Matsumoto, K. Mitsuhara, A. Visikovskiy, T. Akita, N. Toshima and Y. Kido, *Nucl. Instrum. Methods Phys. Res., Sect. B*, 2010, **268**, 2281–2284.
28 P. L. Grande, A. Hentz, R. P. Pezzi, I. J. R. Baumvol and G. Schiwietz, *Nucl. Instrum. Methods Phys. Res., Sect. B*, 2007, **256**, 92–96.
29 R. P. Pezzi, P. L. Grande, M. Copel, G. Schiwietz, C. Krug and I. J. R. Bauravol, *Surf. Sci.*, 2007, **601**, 5559–5570.
30 R. P. Pezzi, C. Krug, P. L. Grande, E. B. O. da Rosa, G. Schiwietz and I. J. R. Baumvol, *Appl. Phys. Lett.*, 2008, **92**, 164102.
31 E. W. M. Born, *Principles of optics: electromagnetic theory of propagation, interference and diffraction of light*, 1997.
32 D. Stroud, *Phys. Rev. B: Solid State*, 1975, **12**, 3368–3373.